Electronic Supplementary Material (ESI) for Journal of Materials Chemistry A.

A high-tap-density nanosphere-assembled microcluster to simultaneously enable high gravimetric, areal and volumetric capacities: A case study of TiO_2 anode

Baisong Chang[a,c], Jinping Liu[a,b], Guangyan Qing[a], and Taolei Sun*[a,b]

[a] State Key Laboratory of Advanced Technology for Materials Synthesis and Processing, Wuhan University of Technology, Wuhan 430070, PR China, E-mail: suntaolei@iccas.ac.cn.

[b] School of Chemistry, Chemical Engineering and Life Science, Wuhan University of Technology, Wuhan 430070, PR China.

[c] State Key Laboratory of Molecular Engineering of Polymers, Fudan University, Shanghai 200433, PR China.

Keywords: Bioinspired synthesis, pomegranate-like TiO_2, microcluster, high-tap-density, high-energy anodes

Corresponding author: Taolei Sun, E-mail: suntl@whut.edu.cn.

Supplementary spectra and images

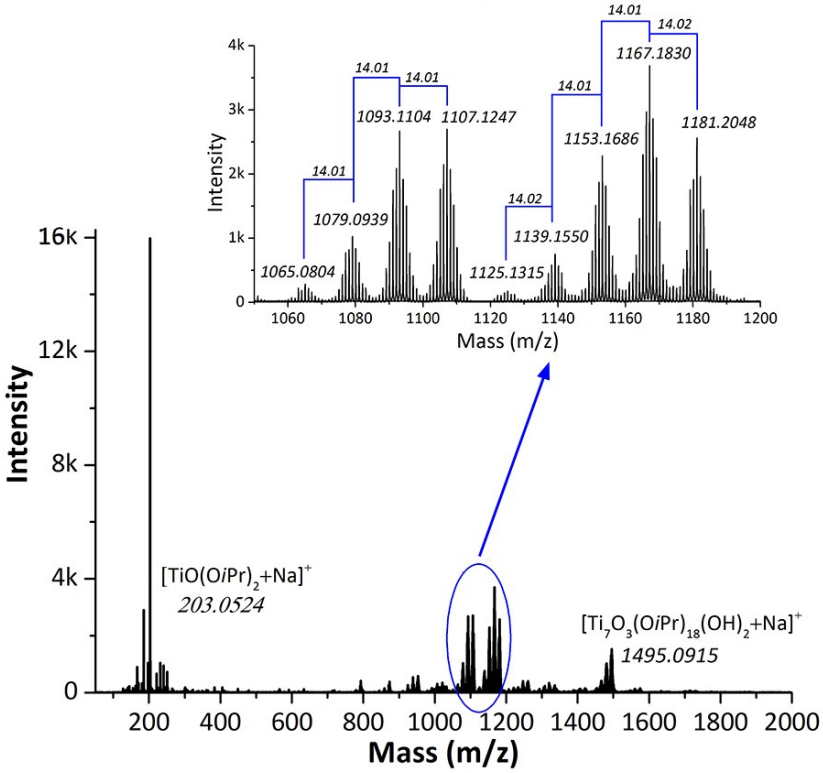

Fig. S1. The mass spectrum of TIP diluted in ethanol as a control. MS analysis was carried out on the electrospray hybrid quadrupole time-of-flight mass spectrometer microTOF-Q (Bruker-Daltonik, Germany) equipped with the electrospray ionization (ESI) ion source. The ESI capillary potential was kept at 4500 V (+) ion mode and the sample was continuously introduced into the source at a rate of 5 µL min^{-1}. A flow of drying N_2 (180 ^oC, 6 L min^{-1}) assisted evaporation of the solvent. The data were collected with a mass range of m/z 50-2000.

The enlarged mass spectra in inset was employed to identify the molecular species. We found that the type of organic solvent used to dissolve TIP played a profound influence on its intrinsic chemical compositions. ESI-MS spectrum of TIP that was dissolved in ethanol showed a dominant peak at m/z 203.0524, corresponding to the adduct ion for $[TiO(OiPr)_2+Na]^+$. It should be noted that another Ti source containing 6-7 Ti atoms was also clearly observed, for example $[Ti_7O_3(OiPr)_{18}(OH)_2+Na]^+$ adducts with a maximum m/z intensity at 1495.0915. Most interestingly, it was possible to demonstrate the existence of different titanium species originating from the exchange between ethanol and the -O*i*Pr group (m/z range from 1050 to 1200) (inset in Fig. S1). The fixed decrease of 14.01 m/z unit was a convincing result that confirmed a step by step substitution of -O*i*Pr ligand (up to four) through $-OCH_2CH_3$ group of ethanol solvent according to the eqn (1):

$$Ti(OiPr)_4 + x\,CH_3CH_2OH \rightarrow Ti(OiPr)_{4-x}(OCH_2CH_3)_x + x\,iPrOH \quad (1)$$

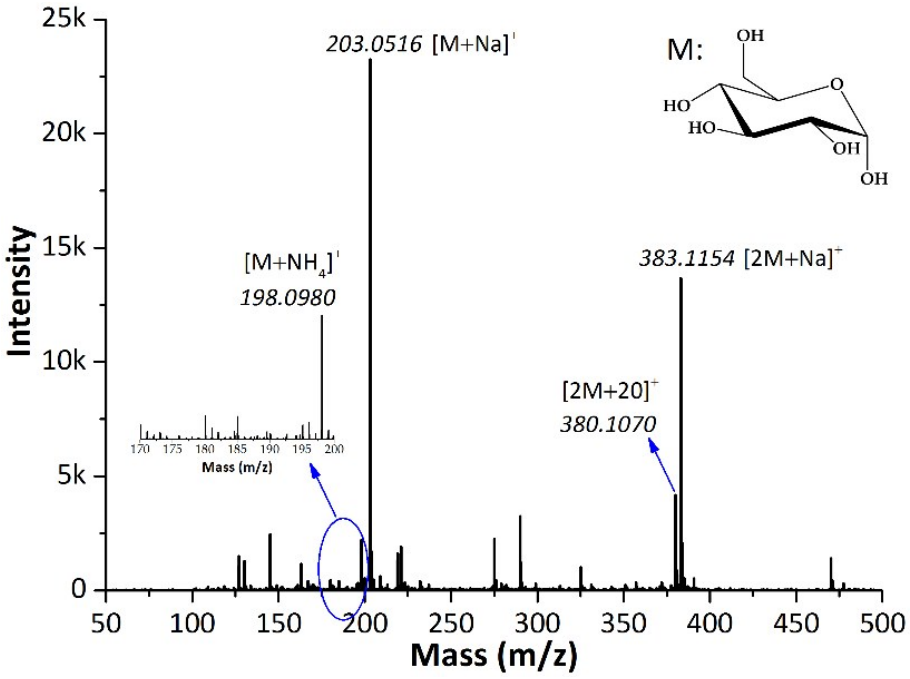

Fig. S2. Mass spectrum of glucose in a positive ion mode. For pure glucose, the abundance of $[M+Na]^+$ adduct of at m/z 203.0516 was the most probable species present, which gave rise to a substantial contrast to GlcN with respect to the type of ions signals. For example, the positive electrospray ionization of GlcN mainly produced protonated a molecular ion of $[M+H]^+$ at m/z 180.0867 (Fig. 1b). The difference in ion signals could serve as a characteristic index to evaluate whether the $-NH_2$ group was successfully connected onto glucose molecules or not.

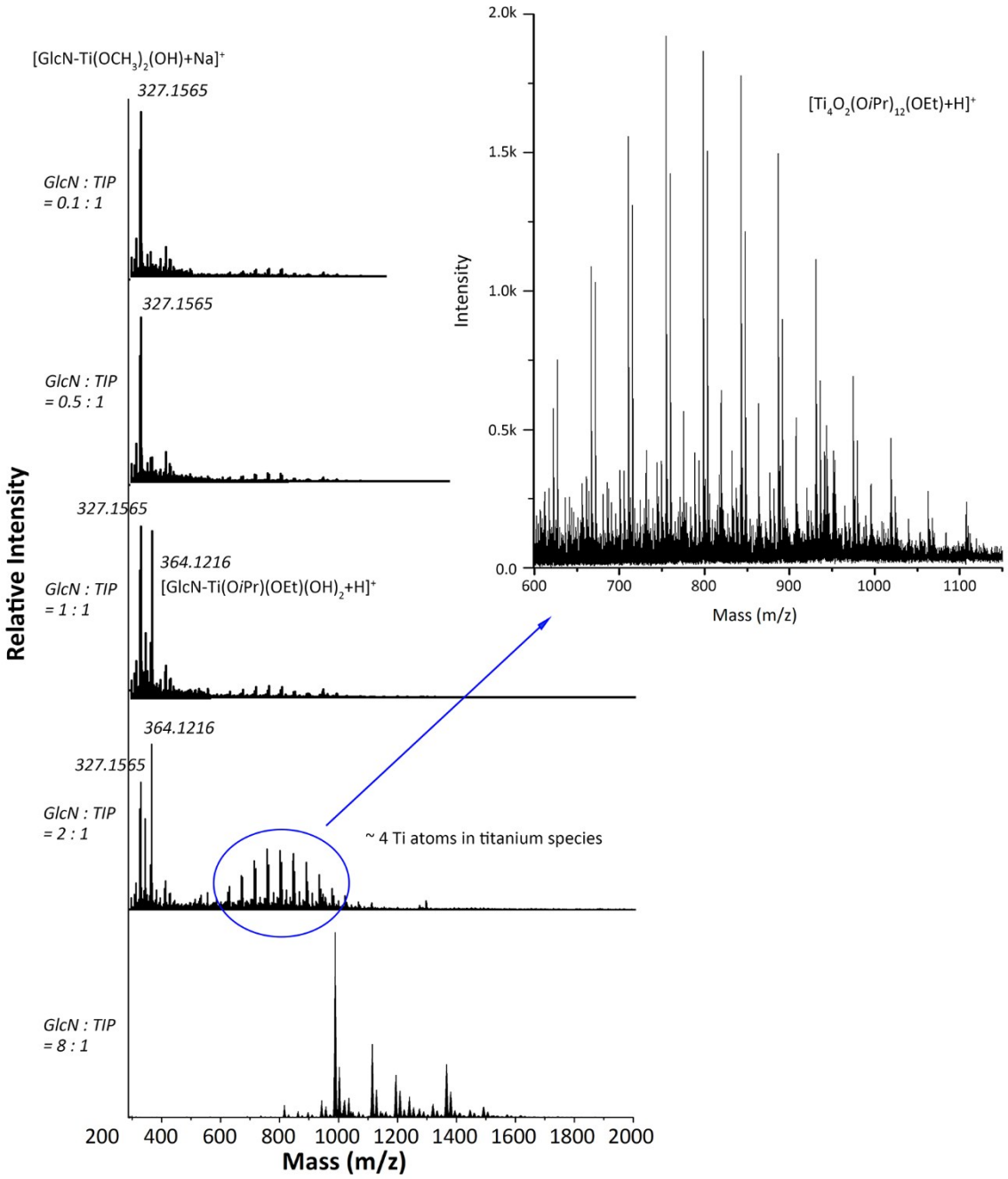

Fig. S3. The molar ratio between GlcN and TIP indeed played a decisive contribution in regulating the purity of Ti species.

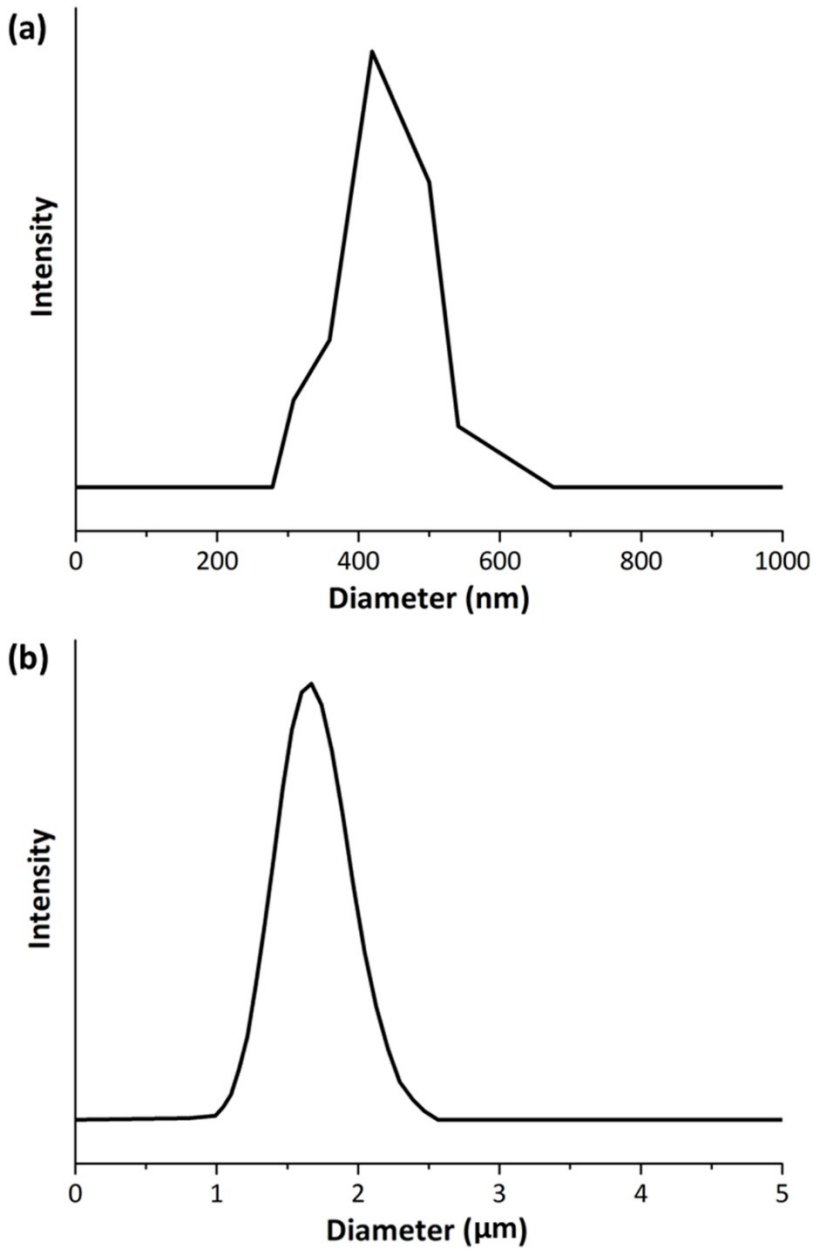

Fig. S4. In aqueous solution with a pH value of 7.4, hydrodynamic diameter of the amorphous TiO_2 microspheres prepared by different mass ratios of HDA/P123/GlcN: (a) 0/0/100% and (b) 24.9/28.7/46.4%. DLS data revealed that the integration of organic additives at an optimum mass ratio would have the greatest influence on the properties of amorphous TiO_2 microsphere. The TiO_2 in (a) exhibited a large size polydispersity index (> 0.3). After dispersed them in water for about 1 day, severe agglomeration and precipitation could be observed. However, the microspheres (b) had a low size polydispersity index (<0.1) and were stable for several months. Such TiO_2 sample was well dispersed without any sedimentation in a longer period.

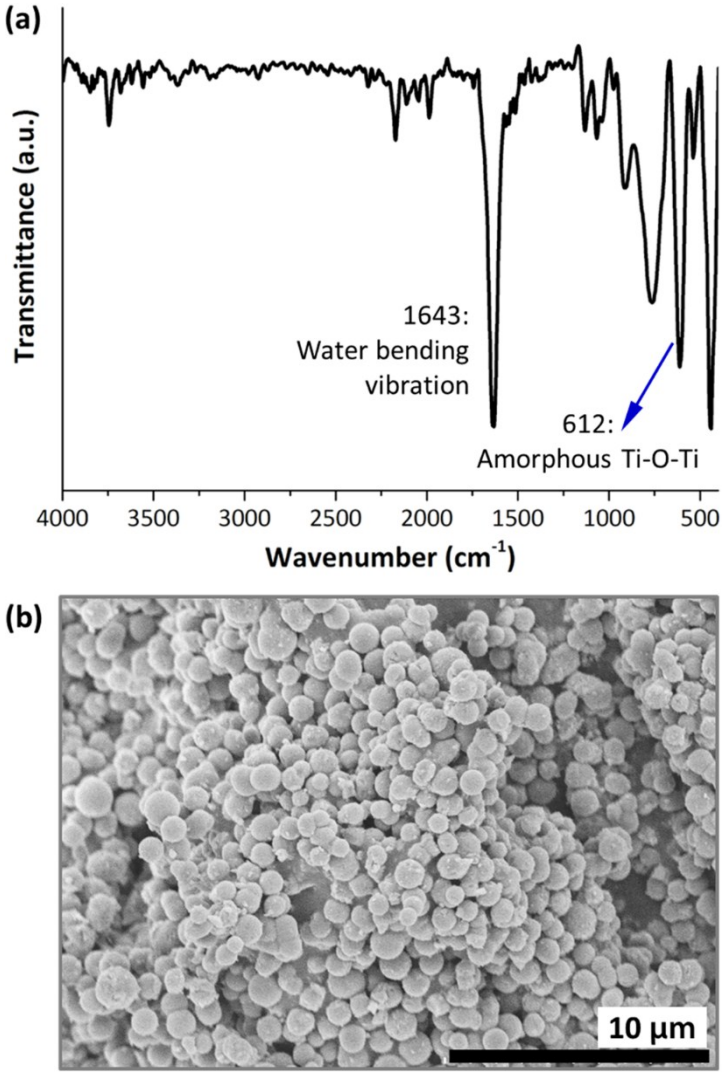

Fig. S5. (a) FTIR spectrum and (b) SEM image of the amorphous blank TiO_2 microspheres prepared without any organic templates. The reaction recipe only contained 2.2 mL of TIP, 0.4 mL of KCl solution (0.1 M) and 100 mL of Isopropanol.

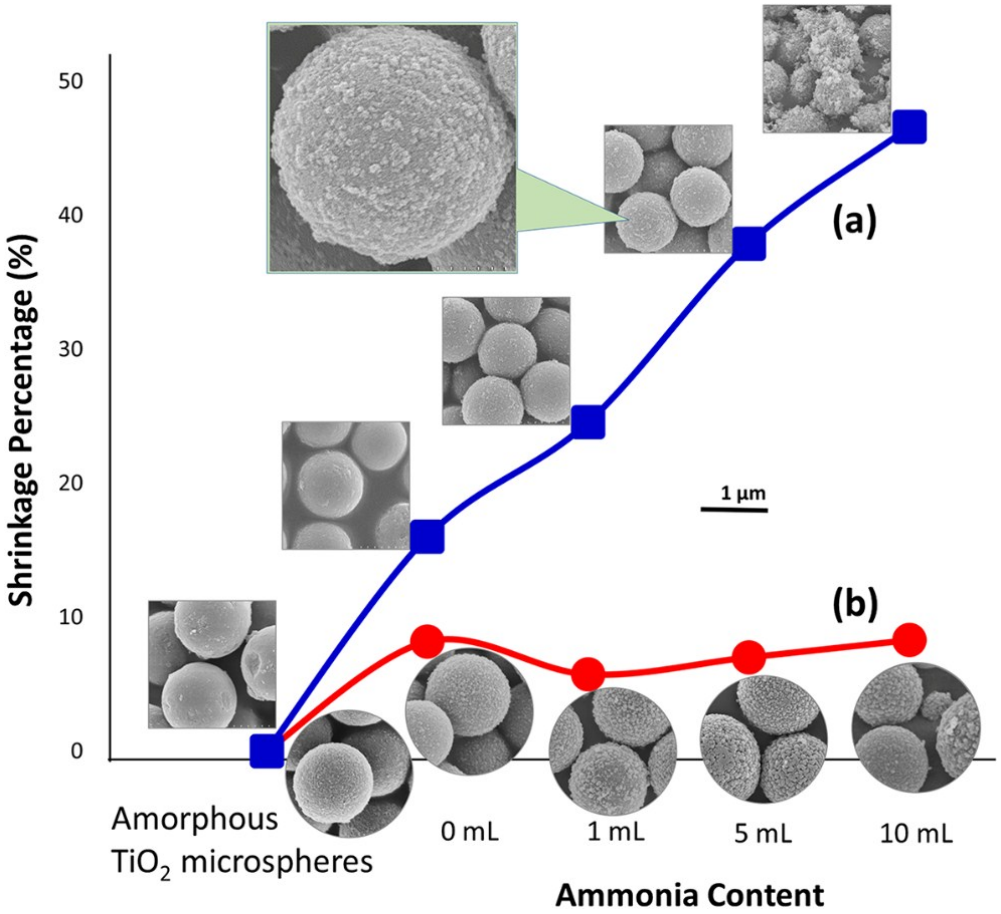

Fig. S6. Schematic diagram displaying the variations (e.g., size shrinkage and surface morphology evolution) of hydrothermally-treated amorphous TiO_2 microspheres with different mass ratios of HDA/P123/GlcN: 100/0/0% (blue curve) and 24.9/28.7/46.4% (red curve). Hydrothermal treatment was carried out in a Teflon-lined autoclave (50 mL) at 160 ^oC for 8 h. The amorphous TiO_2 microspheres were ultrasonically dispersed into a mixture adopting different relative amounts of ammonia, water, and ethanol (volume fraction of 0/10/20, 1/9/20, 2/8/20, 5/5/20, and 10/0/20 mL, respectively), keeping the total solvent volume constant.

To improve the porosity of TiO_2 crystallites, one popular method is to hydrothermally treat amorphous TiO_2 materials prior to calcination.[1] In a particular condition, for example a supercritical fluid that is formed in the autoclave at elevated pressure and temperature, amorphous TiO_2 materials exhibit a relatively high reactivity and mobility toward etching and reconstructions. Such self-ordering reactions through the chemical dissolution possibly brought the spiky core/shell, yolk/shell, hollow, porosity, and even entirely broken structures.[2, 3]

In view of substantial crystal densification, growth, and fusion of TiO_2 in the hydrothermal process, it was not surprising to observe a structural shrinkage in most reported research. For example, high-quality mesoporous TiO_2 microspheres designed by Caruso et al.[4] had a distinct shrinkage of 28% in diameter as compared to our unusual data of 8.3% in a

similar hydrothermal condition (Fig. S6b). To further experimentally confirm this difference, a control of TiO_2 amorphous microspheres prepared by only HDA was conducted. Increasing ammonia concentrations led to a distinct reduction in the size of TiO_2 microspheres (shown in Fig. S6a). Taking the sample hydrothermally-treated in 5 mL of ammonia as an example, the size decreased from 1.07 μm of its starting microsphere to 0.69 μm. A clear shrinkage as high as 36% in diameter was reached. It was a convincing evidence that even at the ammonia amount of 10 mL, GlcN additive could perform specific contribution in inhibiting the micro-structural shrinkage as phase transformation occurred. Nonetheless, when 10 mL of ammonia was added into hydrothermal treatments, the reaction of Ostwald ripening was largely activated, and therefore it can produce a few byproducts besides granular normal microsphere, e.g., irregular nano-sized aggregate.

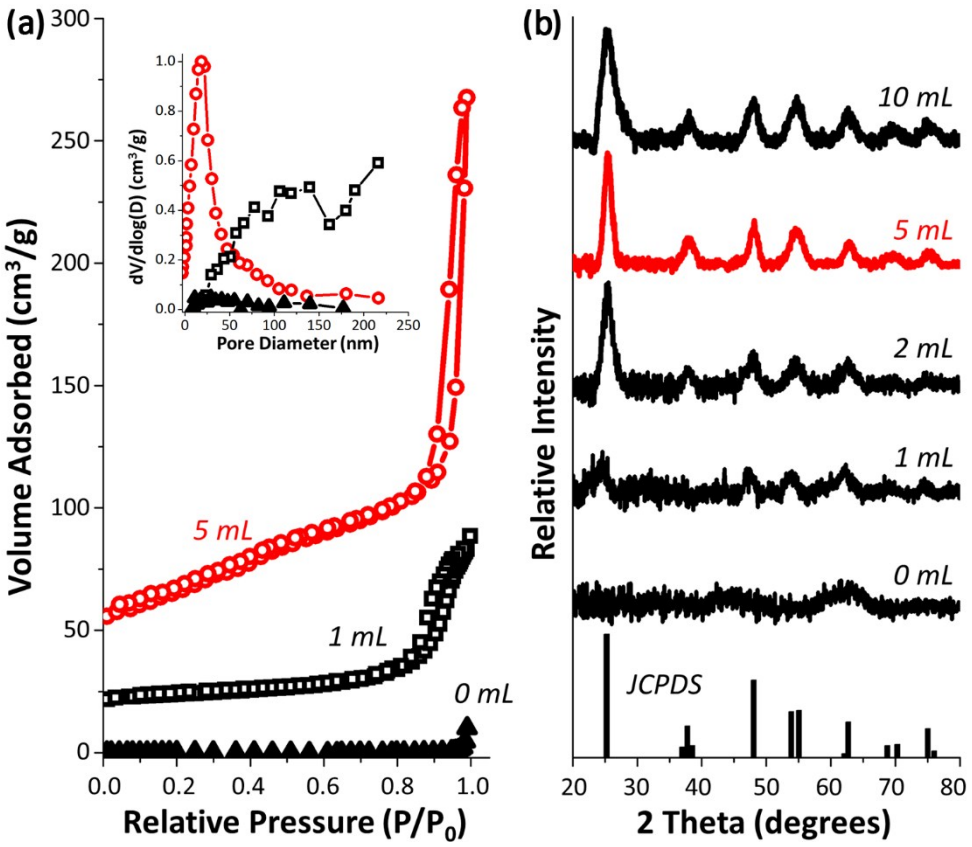

Fig. S7. The hydrothermally-treated amorphous microspheres using the mass ratio of HDA/P123/GlcN at 24.9/28.7/46.4% as a function of ammonia contents: 0, 1, 2, 5 and 10 mL. To understand the structural evolution from smooth precursors to eroded urchin-like titanium counterparts, the crystallization processes for the samples treated with different ammonia contents were investigated by (a) N_2 adsorption-desorption isotherms (inset: pore size distribution; To avoid the overlap of BET isotherms, only three representative curves of hydrothermally-treated samples were given) and (b) XRD analysis.

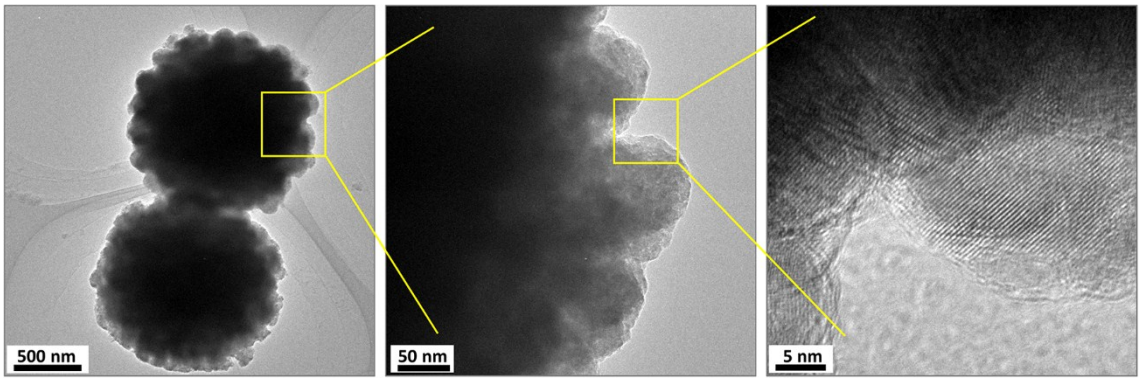

Fig. S8. The synthesis recipe without the use of GlcN always generated solid mesoporous TiO_2 microsphere (denoted as M-TiO_2) after hydrothermal and calcined reactions.

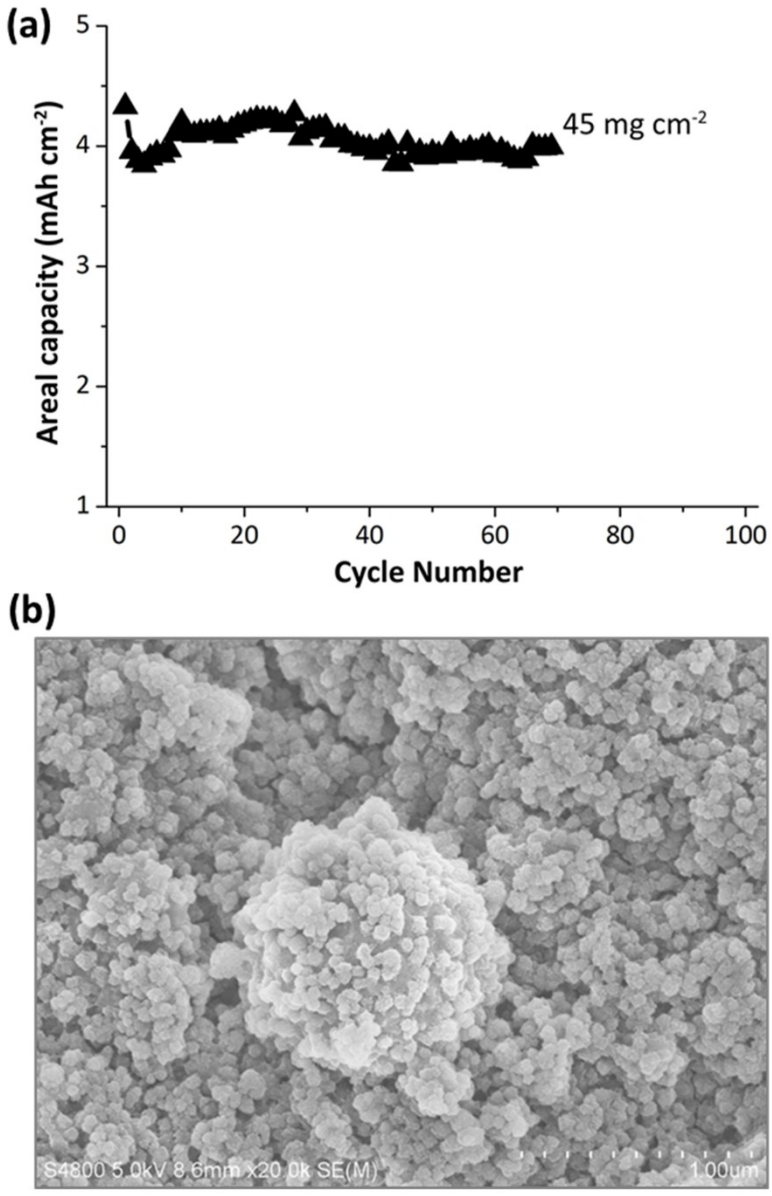

Fig. S9. (a) Cycling performance of pomegranate-like cluster anode with an areal mass loading at 45 mg cm^{-2}. This anode was first cycled at 0.2 C for the first three three cycles and 5 C for the later cycles. (b) The SEM image of pomegranate-like cluster anodes with an areal mass loading at 45 mg cm^{-2} after 1000 cycles at 5 C.

Table S1. Summary of the state-of-the-art gravimetric capability of titanium oxide-based anode materials for lithium-ion batteries (normalized 1C = 335 mA g^{-1}).

References	Materials	Cycle gravimetric capability (mAh g^{-1})		Cycles	Current rate	Rate gravimetric capability (mAh g^{-1})	
		Initial	End			Initial	End
This work	**A high-tap-density microcluster consisting of carbon-conformal hollow TiO_2 nanosphere**	**251**	**197**	**1000**	**1C**	**260@0.1C**	**238@0.2C**
		189	**160**	**1000**	**5C**	**220@0.5C**	**199@1C**
		176	**145**	**1000**	**10C**	**178@2.5C**	**150@10C**
Nano Lett., **2018**, *18*, 336	Three-dimensional TiO_2/Graphene Hybrid	140	150	2000	2C	210@0.1C	72@10C
J. Phys. Chem. B, **2018**, *122*, 972	Carbon nanotube@TiO_2 nanowires	170	150	100	0.06C	80@0.3C	50@1.5C
J. Mater. Chem. A, **2018**, *6*, 1196	TiO_2-B microspheres	220	202	100	5C	216@0.5C	181@10C
J. Mater. Chem. A, **2018**, *6*, 1017	MXenes-derived TiO_2-graphene nanosheet	105	87	8000	3C	181@0.3C	79@6C
J. Alloy. Compd., **2018**, *731*, 844	Mesoporous TiO_2 nanofiber bundles	130	141	500	0.5C	155@0.3C	72@4.8C
ChemSusChem, **2018**, *11*, 299	Single-crystal $H_2Ti_{12}O_{25}$ nanorods	193	175	200	5C	220@0.5C	150@10C
Adv. Funct. Mater., **2017**, *27*, 1703270	Anatase TiO_2@TiO_2(B) microspheres	180	175	500	0.5C	220@0.1C	110@10C
Adv. Energy Mater., **2017**, *7*, 1602291	TiO_2 inverse opal	320	138	1000	0.22C	170@0.4C	130@1.3C
J. Mater. Chem. A, **2017**, *5*, 24380	Mesoporous carbonaceous/TiO_2	150	140	50	1C	180@0.2C	147@1.7C
J. Mater. Chem. A, **2017**, *5*, 23853	Hollow TiO_2-rGO nanocomposites	138	133	800	2.8C	247@0.1C	105@11C
J. Mater. Chem. A, **2017**, *5*, 20651	N-doped anatase TiO_2 nanotubes	\	\	\	\	190@0.07C	78@7.5C
J. Mater. Chem. A, **2017**, *5*, 11764	N-doped C-coated $LiTi_2(PO_4)_3$	125	120	100	0.5C	126@0.08C	62@8.2C

J. Mater. Chem. A, **2017**, *5*, 4359	TiO_2 spheres with hierarchical pores	189	167	100	0.5C	233@0.05C	88@2.5C
ACS Appl. Mater. Interfaces, **2017**, *9*, 36828	Oriented TiO_2 nanotubes	143	132	300	0.05C	172@0.02C	94@5C
ACS Appl. Mater. Interfaces, **2017**, *9*, 35917	TiO_2-B and anatase dual-phase nanowires	180	126	2000	30C	225@0.5C	140@30C
ACS Appl. Mater. Interfaces, **2017**, *9*, 20491	Interpenetrated network of Graphitic carbon/TiO_2	150	140	1000	3C	216@0.3C	123@5.9C
ACS Appl. Mater. Interfaces, **2017**, *9*, 4649	Nanosheets consisting of spinel $Li_4Ti_5O_{12}$ and rutile TiO2 lamellas	133	125	500	25C	178@0.5C	148@10C
Nano Energy, **2017**, *32*, 294	Ti^{3+}-free three-phase $Li_4Ti_5O_{12}/TiO_2$ nanoplates	180	140	1000	12C	175@0.6C	155@24C
RSC Adv., **2017**, *7*, 18745	Spinel $Li_4Ti_5O_{12}$ powder	135	130	99	1C	164@0.05C	132@1C
Electrochim. Acta, **2017**, *255*, 417	N-rich TiO_2@carbon nanosheets	275	136	500	5C	280@0.1C	75@10C
J. Electroanal. Chem., **2017**, *804*, 87	TiO_2 nanorods with rutile@anatase	130	84.7	5000	10C	148@0.5C	93.8@5C
J. Alloy. Compd., **2017**, *721*, 545	$Li_4Ti_5O_{12}$@Carbon fibers	175	173	50	0.5C	175@0.5C	109@10C
J. Am. Chem. Soc., **2016**, *138*, 5916	TiO_2 hollow microsphere	172	170	50	0.05C	175@0.05C	107@5C
Adv. Funct. Mater., **2016**, *26*, 4143	Layered orthorhombic TiO_2@$Ti_3C_2T_X$	120	115	450	2.5C	179@0.25C	96@5C
Chem. Sci., **2016**, *7*, 793	TiO_2 hollow nanosphere	125	110	3000	10C	196@0.5C	113@10C
Nano Energy, **2016**, *21*, 133	Crafting monodisperse $Li_4Ti_5O_{12}$ nanospheres	155	145	500	5C	170@0.25C	135@25C

ACS Appl. Mater. Interfaces, **2016**, *8*, 20040	Three-dimensional branched TiO_2	300	195	200	1C	223@0.5C	123@10C
RSC Adv., **2016**, *6*, 108310	TiO_2@C nanospheres	210	286	200	0.3C	225@0.3C	105@3C
RSC Adv., **2016**, *6*, 95512	Nanostructured $Li_4Ti_5O_{12}$ /PEDOT:PSS	175	169	100	0.25C	168@0.1C	161@5C
Nanoscale, **2016**, *8*, 10928	Hierarchical TiO_2-C heterostructure	200	188	200	0.25C	203@0.1C	103@2.5C
ChemElectroChem, **2016**, *3*, 871	Layer-stacked anatase TiO_2	154	107	10000	3C	242@0.15C	131@6C
J. Mater. Chem. A, **2016**, *4*, 8172	TiO_2-B nanosheets with N-doped carbon	300	210	2200	1.5C	300@0.3C	180@17.9C
J. Mater. Chem. A, **2015**, *3*, 13706	W^{6+} and Br^- co-doped $Li_4Ti_5O_{12}$	155	139	1000	5C	160@0.5C	121@10C
J. Mater. Chem. A, **2015**, *3*, 6455	Single-grain layer anatase TiO_2 nanosheet	110	73	4000	2.5C	200@0.5C	100@5C
ACS Appl. Mater. Interfaces, **2015**, *7*, 10395	Graphene@mesoporous TiO_2@carbon nanosheet	150	125	200	0.6C	90@3C	65@15C
Nano Lett., **2015**, *15*, 2186	TiO_2/graphene/TiO_2 sandwich like nanosheet	252	237	100	0.06C	238@0.1C	175@3C
J. Phys. Chem. C, **2015**, *119*, 3923	Single-Crystalline Anatase TiO_2 Cubes	206	200	100	0.25C	246@0.1C	96@1C
Nanoscale, **2015**, *7*, 17947	Monodisperse TiO_2 microspheres	150	122	500	2.5C	220@0.1C	105@10C
Nanoscale, **2015**, *7*, 13898	TiO_2 microfibers@N doped C composites	130	125	100	5C	200@0.5C	125@5C
Nanoscale, **2015**, *7*, 12979	Yolk-shell TiO_2 porous microspheres	120	113	100	5C	237@0.5C	117@5C

Table S2. Summary of the state-of-the-art areal capability of titanium oxide-based anode materials for lithium-ion batteries.

References	Materials	Cycle areal capability (mAh cm^{-2})		Cycles	Mass loading of active materials (mg cm^{-2})	Current density (mA cm^{-2})
		Initial	End			
This work	**A high-tap-density microcluster consisting of carbon-conformal hollow TiO_2 nanosphere**	**5.01**	**4.79**	**1000**	**23.7**	**26.0**
		3.69	**3.20**	**1000**	**15.6**	**26.0**
		2.21	**1.80**	**1000**	**8.2**	**26.0**
Energy Environ. Sci., **2017**, *10*, 580	Yolk-shell Si@TiO_2 nanoclusters	3.1	2.0	50	2.1	0.7
Adv. Mater., **2017**, *29*, 1700523	Silicon@amorphous TiO_2 nanoparticles	2.25	1.07	200	0.62	0.26
J. Mater. Chem. A, **2017**, *5*, 11764	Nitrogen-doped carbon-coated $LiTi_2(PO_4)_3$	1.44	1.32	80	10	1.38
J. Alloy. Compd., **2017**, *712*, 90	Anatase TiO_2 nanotube	0.088	0.075	50	\	0.05
J. Electrochem. Soc., **2017**, *164*, E3114	TiO_2 columnar nanostructures	\	0.075	100	0.43	0.01
		0.085	0.071	100	0.43	0.14
		\	0.069	100	0.43	0.28
		\	0.030	100	0.43	0.70
J. Power Sources, **2017**, *345*, 50	Nanoengineered TiO_2 thick films	3.35	2.28	30	18.0	6.03
		2.88	2.12	30	15.5	5.19
		2.25	1.77	30	12.5	4.18
		1.89	1.41	30	10.5	3.52
		1.25	0.95	30	3.4	1.14
		0.61	0.47	30	3.0	1.01
Adv. Funct. Mater., **2017**, *27*, 1703538	SiO_2/TiO_2 composite film	1.73	0.85	50	\	0.05
		0.75	0.52	50	\	0.1
		0.66	0.49	50	\	0.2
		0.51	0.39	50	\	0.3
		0.47	0.24	50	\	0.5
Materials, **2017**, *10*, 678	Ternary CNTs@TiO_2/CoO nanotubes	1.24	0.31	50	< 1.1	0.05

J. Mater. Chem. A, **2016**, *4*, 5542	TiO_2-SnO_2 nanotubes	0.41	0.41	5	1.91	1.01
		1.61	0.49	400	1.91	0.50
		0.70	0.66	5	1.91	0.25
		0.85	0.78	5	1.91	0.10
		1.13	1.00	5	1.91	0.05
J. Mater. Chem. A, **2016**, *4*, 7398	Coaxial TiO_2-carbon nanotube sponges	\	4.4	30	19.5	1.95
		\	4.1	30	18.2	1.82
		\	3.7	30	16.4	1.64
		\	1.6	30	7.1	0.71
		\	1.4	30	6.2	0.62
J. Mater. Chem. A, **2016**, *4*, 10593	TiO_2 nanotrees	0.32	0.27	50	\	0.1
		0.25	0.21	5	\	0.5
		0.19	0.15	400	\	1.0
		0.15	0.14	5	\	2.0
		0.01	0.01	5	\	5.0
		0.07	0.07	5	\	10.0
Electrochim. Acta, 2016, 198, 56	Anodic TiO_2 nanotubes	\	0.63	\	2.4	0.02
ACS Appl. Mater. Interfaces, **2016**, *8*, 16670	Anodized Ti_3SiC_2	0.31	0.23	60	\	0.5
		0.32	0.32	10	\	0.3
		0.46	0.38	25	\	0.2
J. Power Sources, **2015**, *282*, 187	Three-dimensional porous TiO_2/carbon fiber	\	3.90	\	54.1	1.8
		\	2.49	\	54.1	18.1
		\	1.15	\	54.1	36.2
		\	2.98	\	40.2	1.3
		\	2.03	\	40.2	13.4
		\	1.30	\	40.2	26.8
		\	1.50	\	21.9	0.73
		\	1.02	\	21.9	7.3
		\	0.91	\	21.9	14.6

Electrochim. Acta, **2015**, *163*, 246	Two-dimensional metal carbides	7.45	1.7	50	50	1.5
		8.51	2.2	50	35	1.5
		7.14	2.0	50	18	1.5
	Two-dimensional metal/carbon composite	16.0	4.9	50	50	1.5
		6.0	2.8	50	35	1.5
		7.7	2.1	50	18	1.5

Table S3. Summary of the state-of-the-art volumetric capability of titanium oxide-based anode materials for lithium-ion batteries (normalized 1C = 335 mA g^{-1}).

References	Materials	Cycle volumetric capability (mAh cm^{-3})		Cycles	Mass loading of active materials (mg cm^{-2})	Current rate
		Initial	End			
This work	**A high-tap-density microcluster consisting of carbon-conformal hollow TiO_2 nanosphere**	**970**	**954**	**10**	**8.2**	**5.0C**
		1058	**1019**	**5**	**15.6**	**0.1C**
		973	**956**	**5**	**15.6**	**0.2C**
		955	**931**	**5**	**15.6**	**0.5C**
		942	**900**	**5**	**15.6**	**1.0C**
		919	**885**	**5**	**15.6**	**2.5C**
		871	**856**	**1000**	**15.6**	**5.0C**
		804	**786**	**10**	**23.7**	**5.0C**
ChemSusChem, **2018**, *11*, 299	Single-crystal $H_2Ti_{12}O_{25}$ nanorods	497	325	10	3.7	0.3C
		320	303	100	3.7	0.6C
		293	283	10	3.7	1.2C
		250	258	10	3.7	3.0C
		239	222	10	3.7	6.0C
		163	160	10	3.7	12.0C
Energy Environ. Sci., **2017**, *10*, 580	Yolk-shell Si@TiO_2 nanoclusters	\	930	100	2.1	0.5C
J. Mater. Chem. A, **2017**, *5*, 330	Titanium phosphate thin films	335	330	100	≈ 2.8	1C
Nano Energy, **2017**, *31*, 377	A two-layer anode: porous TiO_2/non-porous TiO_2	450	440	5	2.9	0.1C
		370	360	5	2.9	0.5C
		255	255	5	2.9	1.0C
		125	120	5	2.9	2.0C
		75	70	5	2.9	4.0C
Adv. Funct. Mater., **2017**, *27*, 1703538	SiO_2/TiO_2 composite film	841	708	50	\	0.1C
		624	433	50	\	0.5C
		549	408	50	\	1.0C
		424	324	50	\	2.0C
		391	199	50	\	4.0C

Sci China Mater., **2017**, *60*, 304	Mesoporous TiO_2 submicrospheres	118	105	5	24	0.1C
		95	90	5	24	0.2C
		78	75	5	24	0.5C
		70	60	5	24	1.0C
Adv. Funct. Mater., **2016**, *26*, 4143	Layered orthorhombic TiO_2@$Ti_3C_2T_X$	355	\	1	21	0.2C
		274	\	1	21	1.0C
	Layered orthorhombic TiO_2@$Ti_3C_2T_X$	141	\	1	2.65	0.25C
		113	\	1	2.65	1.0C
J. Mater. Chem. A, **2016**, *4*, 10593	TiO_2 nanotrees	\	330	50	\	≈ 0.3C
Nano Energy, **2016**, *21*, 133	Crafting monodisperse $Li_4Ti_5O_{12}$ nanospheres	198	193	5	2.0	0.05C
		187	190	5	2.0	0.25C
		178	178	5	2.0	0.5C
		175	175	5	2.0	1.0C
		171	170	5	2.0	2.5C
		170	159	500	2.0	5.0C
		156	160	5	2.0	10C
		155	155	5	2.0	15C
		143	150	5	2.0	25C
		115	108	5	2.0	40C
Chemelectrochem, **2016**, *3*, 1301	Beaded stream-like $Li_4Ti_5O_{12}$ nanoparticles	340	300	5	1.25	0.08C
		265	260	5	1.25	0.21C
		270	250	500	1.25	0.42C
		250	248	5	1.25	0.84C
		246	225	500	1.25	2.1C
		220	215	5	1.25	4.2C
		210	198	5	1.25	8.4C
Electrochim. Acta, **2016**, *202*, 203	Hierarchical rutile TiO_2 with mesocrystalline structure	412	231	100	≈ 1.7	0.3C
		209	207	5	≈ 1.7	0.6C
		171	165	5	≈ 1.7	1.5C
		141	138	5	≈ 1.7	3.0C
		113	109	5	≈ 1.7	6.0C
Adv. Sci., **2015**, *2*, 1500070	Mesoporous TiO_2 nanowire bundles	295	283.6	100	≈ 3.2	0.5C

Int. J. Electrochem. Sci., **2015**, *10*, 8993	TiO_2@carbon nanostructure	160	42.6	10	0.6	0.15C
		40.3	36.4	10	0.6	0.3C
		35.8	31.2	10	0.6	0.6C
		27.3	23.4	10	0.6	1.5C
J. Power Sources, **2015**, *282*, 187	Three-dimensional porous TiO_2/carbon fiber	39.0	\	1	40.2	0.1C
		27.5	\	1	40.2	1.0C
		21.2	\	1	40.2	2.0C
J. Power Sources, **2015**, *273*, 923	TiO_2(B) secondary microspheres	467	\	1	2.0	0.18C
		450	\	1	2.0	0.44C
		445	\	1	2.0	0.89C
		435	\	1	2.0	1.78C
		430	\	1	2.0	2.67C
		425	\	1	2.0	3.56C
		422	\	1	2.0	4.44C
		416	\	1	2.0	7.11C
		410	\	1	2.0	8.89C
		405	\	1	2.0	13.3C
		387	\	1	2.0	17.8C
	Needle-like TiO_2(B)	460	\	1	2.0	0.18C
		455	\	1	2.0	0.44C
		438	\	1	2.0	0.89C
		405	\	1	2.0	1.78C
		398	\	1	2.0	2.67C
		376	\	1	2.0	3.56C
		355	\	1	2.0	4.44C
		330	\	1	2.0	7.11C
		310	\	1	2.0	8.89C
		27**5**	\	1	2.0	13.3C
		248	\	1	2.0	17.8C

References:

1 W. Li, Z. Wu, J. Wang, A. Elzatahry and D. Zhao, *Chem. Mater.*, 2014, **26**, 287-298.

2 L. Cao, D. Chen and R. A. Caruso, *Angew. Chem. Int. Ed.*, 2013, **52**, 10986-10991.

3 K. Lee, A. Mazare and P. Schmuki, *Chem. Rev.*, 2014, **114**, 9385-9454.

4 D. Chen, F. Huang, Y. Cheng and R. A. Caruso, *Adv. Mater.*, 2009, **21**, 2206-2210.